

Fabrication of localized diamond-filled copper structures via selective laser melting and spark plasma sintering

Ramin Rahmani^{a,b,c,*}, Javad Karimi^{c,d}, Nikhil Kamboj^{c,e,f}, Rahul Kumar^{c,g}, Miha Brojan^h, Adam Tchórzⁱ, Grzegorz Skrabalakⁱ, Sérgio Ivan Lopes^{a,j}

^a CiTin– Centro de Interface Tecnológico Industrial, 4970-786 Arcos de Valdevez, Portugal

^b proMetheus– Instituto Politécnico de Viana do Castelo (IPVC), 4900-347 Viana do Castelo, Portugal

^c Tallinn University of Technology, Department of Mechanical and Industrial Engineering, Ehitajate tee 5, 19086 Tallinn, Estonia

^d BIAS– Bremer Institut für angewandte Strahltechnik GmbH, Klagenfurter Straße 5, Bremen 28359, Germany

^e Department of Mechanical and Materials Engineering, University of Turku, FI-20500 Turku, Finland

^f TCBC– Turku Clinical Biomaterials Centre, Department of Biomaterials Science, Faculty of Medicine, Institute of Dentistry, University of Turku, FI-20014 Turku, Finland

^g AC2T Research GmbH, Viktor Kaplan-Straße 2/c, 2700 Wiener Neustadt, Austria

^h Laboratory for Nonlinear Mechanics, Faculty of Mechanical Engineering, University of Ljubljana, Aškerčeva cesta 6, 1000 Ljubljana, Slovenia

ⁱ Centre of Advanced Manufacturing Technologies, Lukaszewicz Research Network, Krakow Institute of Technology, Zakopiańska 77, 30-418 Kraków, Poland

^j ADiT-Lab, Instituto Politécnico de Viana do Castelo (IPVC), 4900-347 Viana do Castelo, Portugal

ARTICLE INFO

Keywords:

Additive manufacturing
Selective laser melting
Spark plasma sintering
Diamond powder
Copper alloys
Heatsink

ABSTRACT

Selective laser melting (SLM) process is a promising additive manufacturing technique for the fabrication of 3D metallic components with complex geometries. When applied to a porous structure made of a low-alloyed copper, the results show a good producibility and malleability for structures made of CuNi₂SiCr. On the other hand, powder metallurgy proposes spark plasma sintering (SPS) process to introduce diamond particles (resin-bonded micron-size and crystalline with 50 % coating) into a 3D-built copper structure to achieve fast and highly densified fabrication. The present work aims to achieve better positioning, consolidation and densification of the diamond particles at the desired location of the structure, which includes both the lattice and the bulk. This paper studies an additively manufactured diamond-reinforced copper structure developed for fabricating heatsinks by SLM and SPS. These metal-diamond hybrid composites can potentially be used for electro-thermal applications, refractory composites or bio/tribological applications. The demonstrated privileges include i) AM techniques using SLM with low laser power, ii) larger layer thicknesses with higher productivity and iii) rapid fabrication of porous structures with successively applying plasma sintering to fill them with hard materials like diamond particles.

1. Introduction

Selective laser melting (SLM), as a subset of the powder bed fusion (PBF) processes and one of the most promising additive manufacturing (AM) technologies, enables a layer-by-layer fabrication of near-net, complex, and three-dimensional shapes directly from the computer-aided design (CAD) design from a wide range of materials [1]. The procedure can roughly be described relatively simply; as the recoater deposits a layer of powder with a defined thickness from the feeding chamber onto the build plate during the SLM process, a laser beam with the help of a mirror scanner deflector in x-y axis then the powder

particles melt selectively. During the reciprocating motion of the recoater/roller, a new layer of object is produced, and when the built plate moves down after laser irradiation, a new powder layer covers it, and the process repeats until the job finishes and the final 3D structure is built [2,3]. Low production speed, high fixed price for solid materials and limitations in composition of materials are the limitations of the SLM process in comparison to metal injection molding (MIM), however, for small batch prototyping and customized design, SLM is great option rather than MIM [4]. Moreover, the post-processing (chemical, thermal, ultrasonic, blasting, etc.) and focus on the application are crucial to avoid fabrication difficulties, such as unexpected defects and cracks

* Corresponding author at: CiTin– Centro de Interface Tecnológico Industrial, 4970-786 Arcos de Valdevez, Portugal.

E-mail addresses: ramin.rahmani@citin.pt, ramin.rahmaniahranjani@gmail.com (R. Rahmani).

<https://doi.org/10.1016/j.diamond.2023.109916>

Received 10 February 2023; Received in revised form 24 March 2023; Accepted 6 April 2023

Available online 10 April 2023

0925-9635/© 2023 Elsevier B.V. All rights reserved.

during 3D printing, unmolten powders, and other long and expensive production processes [5].

On the other hand, modern powder metallurgy (PM) offers a high heating rate (Joule heating), short holding time, surface diffusion for coarser grains, arrangement of particles by uniaxial pressure control, minimization of grain growth (almost theoretical) and programmable sintering/consolidation, called spark plasma sintering (SPS) [6]. Energy savings, the efficiency of the process and vaporization reduction are other advantages of the SPS over the conventional methods. In this process, low voltage and high amperage pulsed direct current is passed through the conductive sample particles (surrounded by graphite die and sheet) which distributes the temperature radially and axially [7,8]. The ability to design customized molds to avoid subtractive post-processing, production of cermet composites with numerous components and the possibility of combining with the SLM are the main advantages of the SPS process [9].

SLM (or laser processing such as cladding) of copper and copper-based alloys is limited due to their high thermal conductivity and reflectivity [10]. To overcome this obstacle, high laser power and relatively large hatch distance are required [11]. Nowadays, 3D printing of pure copper is still facing problems, especially to pronounced heat transfer between the layers [12]. The new experiments in SLM focus on more absorption than reflection, and the present solution, is to use short green light (wavelength ~ 500 nm) compared to infrared light (wavelength ~ 1000 nm) and apply high laser power (~ 1 kW) [13]. In modern PM, SPS provides a better solution for higher densification and even uses Cu as a matrix with other refractory materials for heatsinks and thermal conductivity applications [14,15]. The high virucidal potential of Cu-based materials is another advantage for in-vitro applications, especially in the post-Covid19 era [16,17], including the field of biotribology (advantageous generation of a copper transfer film on the counterpart, which contributes to improved sliding conditions) [18]. Also, in the transition to digitalization and industrial revolutions (both Industry 4.0 and 5.0), the combination of PBF with traditional technologies is crucial [19]. Therefore, the application of PBF and PM technologies using copper and its alloys for the design of novel Human-Machine Interfaces (HMI) is an essential part of Industry 5.0 human-centricity, where AM [20] and bio/tribological materials can be exploited [21].

The superiority of SPS among PM processes lies in its high solidification and near-theoretical densification, while the beneficial properties of SLM in LPBF techniques lie in the uniform distribution of diamond particles in the Cu matrix. Metallic alloys with poor weldability, low immiscibility and high thermal conductivity show poor printability and crack susceptibility in the SLM process, which is a major challenge for a wide range of materials. However, a combination of SLM and SPS techniques could potentially overcome these limitations. The objective of the present work is to provide an overview of the positioning of diamond particles doped/embedded into the lattice/bulk architectures of copper using SLM and SPS techniques. The SPS process provides high densification in the Cu-Di composite, but shape complexity of sample, requires a mold designing. The results of this study can be directed to the thermal conductivity of Cu-Di hybrid composites as heatsinks, face-to-abrasive/impact (wear) surfaces with a desirable diamond content, and impact absorption in antibacterial applications.

2. Materials and methods

2.1. Copper-balanced powders

Pure copper (Sigma-Aldrich, 99.5 wt% metal balance, USA) was chosen to mix with diamond particles and used in the SPS process. However, for SLM processes, flowability and spherical shaping play a crucial role. Therefore, CuNi2SiCr (Eckart TLS GmbH, 96.5 wt% copper balance, Germany) gas-atomized copper-based powders with 10–63 μm size particles, specifically produced for LPBF process, were used. High

surface roughness diamond particles (resin-bonded crystalline RBM—50C, 40–50 μm , from Van Moppes, Swiss, was coated with 50 % copper) was served as a binder in copper diamond mixture. Scanning Electron Microscope (SEM) micrographs of the particles are shown as Fig. 1. CuNi2SiCr powder was applied for 3D printing of heatsink structures during the SLM process, while a mixture of pure copper and RBM-50C (Cu-Di composite) was ball-milled for the use in SPS. The elemental powders were blended for 3 h by a blending machine. To prevent damage to the diamond particles, during the ball milling process, a low rotation speed is used for Cu-Di composite along with zirconia balls (stabilized with yttria).

2.2. SLM and SPS processes

The Realizer SLM®280 device (supplied by SLM-Solutions AG, Germany) was used for CuNi2SiCr structures in the lattice, porous, or heatsink forms with the parameters given in Table 1 and argon gas flow through the build chamber.

In addition, the SPS device (supplied by FCT Systeme GmbH, Germany) with a nitrogen flow glovebox (avoiding oxidation and contamination) and a vacuum chamber (for sintering under uniaxial pressure and controlled temperature-time) was used in our copper-diamond fabrication. Three copper-diamond samples were sintered with identical pressure conditions, but with different times and temperatures (depending on the percentage of diamond particles). SPS parameters for Cu-Di samples are described in the Discussion section. The schematic configuration of SLM and SPS –individually or in combination– is shown in Fig. 2. The percentage of metallic parts (copper alloys in bulk, lattice, scaffold, triply periodic minimal surface, etc.) and their fabrication can be designed in structure SLMed. In contrast, the ceramic parts of composite (diamond particles with/without coating, hard materials, etc.) can be appeared in SPSed binder. Nevertheless, this SLM-SPS combined approach defines distribution of metallic and ceramic parts in the cermet composite.

2.3. X-ray diffraction (XRD) and scanning electron microscope (SEM) characterizations

SLMed 3D-printed CuNi2SiCr structure was compared in terms of dimensional accuracy with three metallic powders which are known and popular in laser PBF technology; namely, 316 L, Ti6Al4V and AlSi10Mg metallic structures. Phase analysis of the Cu-Di composites was measured by X-ray diffraction (D5005 Bruker, USA) operating at $\text{CuK}\alpha 1$ radiation with the range of $20\text{--}120^\circ$ and step of 2θ which is optimized by Rietveld refinement technique. Micro-computed tomography (Micro-CT) scans of the heatsinks superimposed on the CAD design of the heatsinks and the results are presented as color-coded deviation maps using GOM Inspect software (Braunschweig, Germany). For this study, tests are performed by the voxel size of 23.2 μm , 1400 projections (600 ms per each) and X-ray power source of 28.5 W with a reflection target tube [22]. An X-ray micro-topography of the samples was considered for the assessment of defects and pores (with minimum $8 \times 10^{-6} \mu\text{m}^3$ volume pore) in different cross sections using the GE phoenix v|tome|x s240 device and GE Datos software equipped with beam hardening effect. The Hitachi TM3000 Tabletop Scanning Electron Microscope (SEM) equipped with a Deben analyzer was used to observe the microstructure of the samples.

2.4. SLMed heatsink design

The heatsinks were designed using SolidWorks CAD. Two examples with cylindrical pin fins and rectangular plate fins are shown in Fig. 3. To illustrate the printability and densification of alloys, Iron-based 316 L, Aluminum-based AlSi10Mg, Titanium-based Ti6Al4V, and Copper-based CuNi2SiCr cylindrical heatsink were additively manufactured. The diameter of the cylindrical heatsinks was 20 mm and other

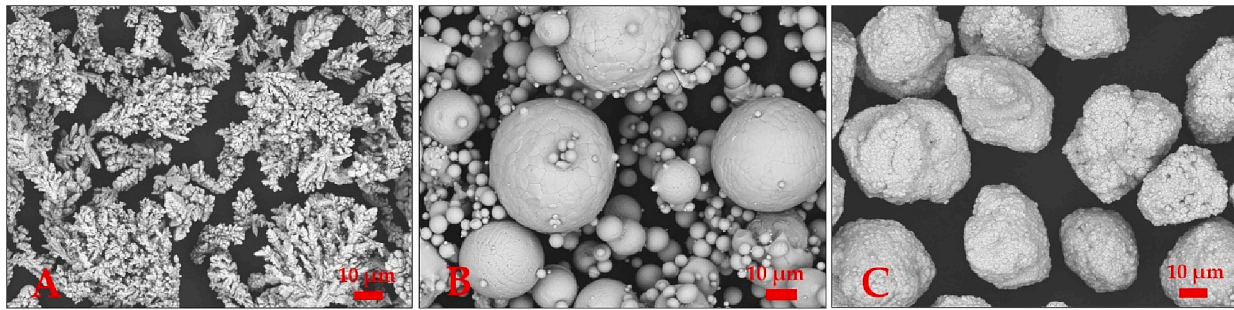


Fig. 1. Powder SEM micrograph A) Pure copper, B) Pre-alloyed gas-atomized spherical-shaped copper-based CuNi2SiCr alloy, and C) Diamond particles with 50 % copper coating (RBM-50C).

Table 1
SLM process parameters.

Process parameters	Unit	Value
Laser power	W	100
Scanning speed	mm/s	1000
Layer thickness	μm	50
Point distance	μm	25
Exposure time	μs	25
Laser current	mA	3000
Laser wavelength	nm	~1060
Overlap rate	%	30
Oxygen level	%	≥0.05

dimensions are mentioned in Fig. 4 and Table 2. The powders used in this study, their producers and specifications, and the particle sizes are listed in Table 3.

2.5. SPSed Cu-Di composites

SPSed Cu-Di hybrid composites with varying diamond content (1/3, 1/2, and 2/3 Di) are fabricated in vacuum chamber with temperature ranging from 780 °C for Cu pure to 860 °C for Cu-2/3 Di. The temperature is determined based on the amount of Cu and is established to prevent copper leakage during the dwell phase. The SPS parameters for the Cu-based samples include a 20 MPa pressure, 100 °C/min ramp rate, and 15 min dwell time. The experiments are repeated three times per

sample to ensure accuracy. The SPS process parameters used here are addressed in [23]. Young’s modulus of Cu-Di composites was measured using the ultrasonic methods (Panamatrix Epoch-3), which is based on the velocity of longitudinal and transverse ultrasonic waves and eliminates the overlapping pulses. Meanwhile, the Cu-Di SPSed samples were polished once for 30 min with P800 abrasive paper, once coarse polishing, and then fine polished to see the if the diamond particles be retained or removed in the matrix even at high abrasively medium. Therefore, it is recommended to use SPS for bulk shapes and binder jetting (BJ) for complex structures, instead of SLM when high densification or precision is required.

3. Results and discussion

This study focuses on pre-alloyed copper alloy CuNi2SiCr. The SEM micrographs of both cylindrical and rectangular heatsinks (representatives of rounded and flat solid structures) are respectively shown in Figs. 5 and 6. Sticked/unmolten powders are more likely to be on the lateral side (at outermost end of the struts) due to the different sizes of powders (10–63 μm), but in the inner parts of the cross-section they are fused and they’re fine due to the proper thermal conductivity/diffusivity (valid for both, the circular and rectangular lateral sides).

Fig. 7 shows micro-CT scan of the AM fins fabricated using the SLM from four different metallic alloys, including 316 L, AlSi10Mg, Ti6Al4V, and CuNi2SiCr. Porosity and densification assessment are good criteria to demonstrate the printability of a structure before mechanical

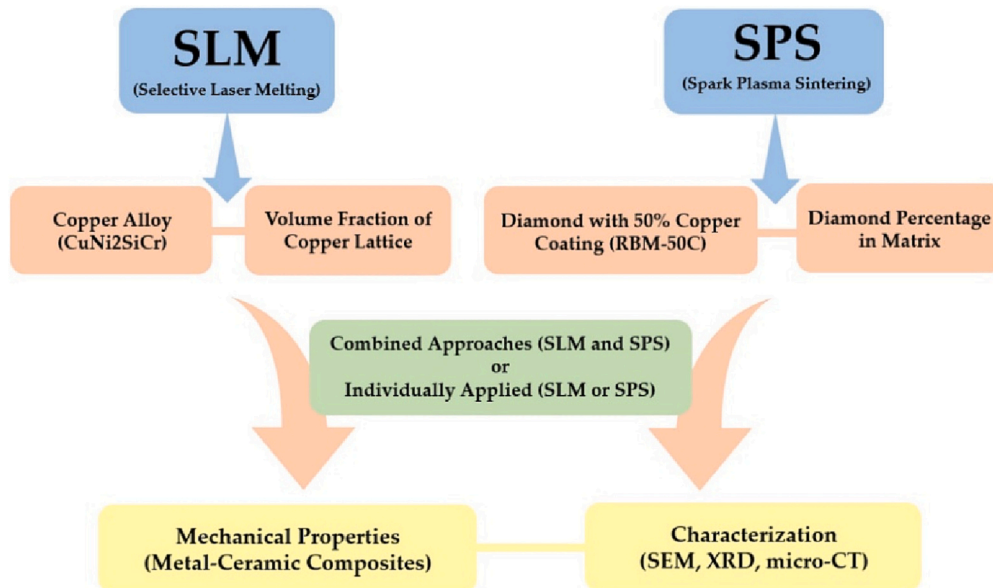


Fig. 2. Schematic configuration of SLM-SPS combined processes.

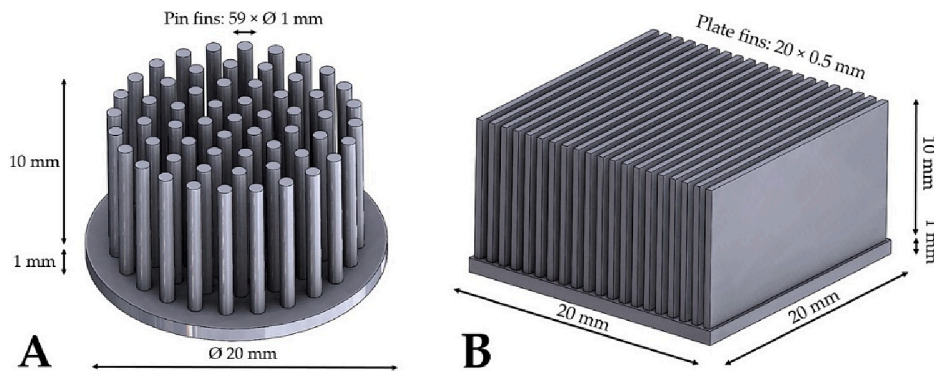


Fig. 3. CAD design and dimensions of the heatsink, A) Cylindrical pin fins, and B) Rectangular plate fins.

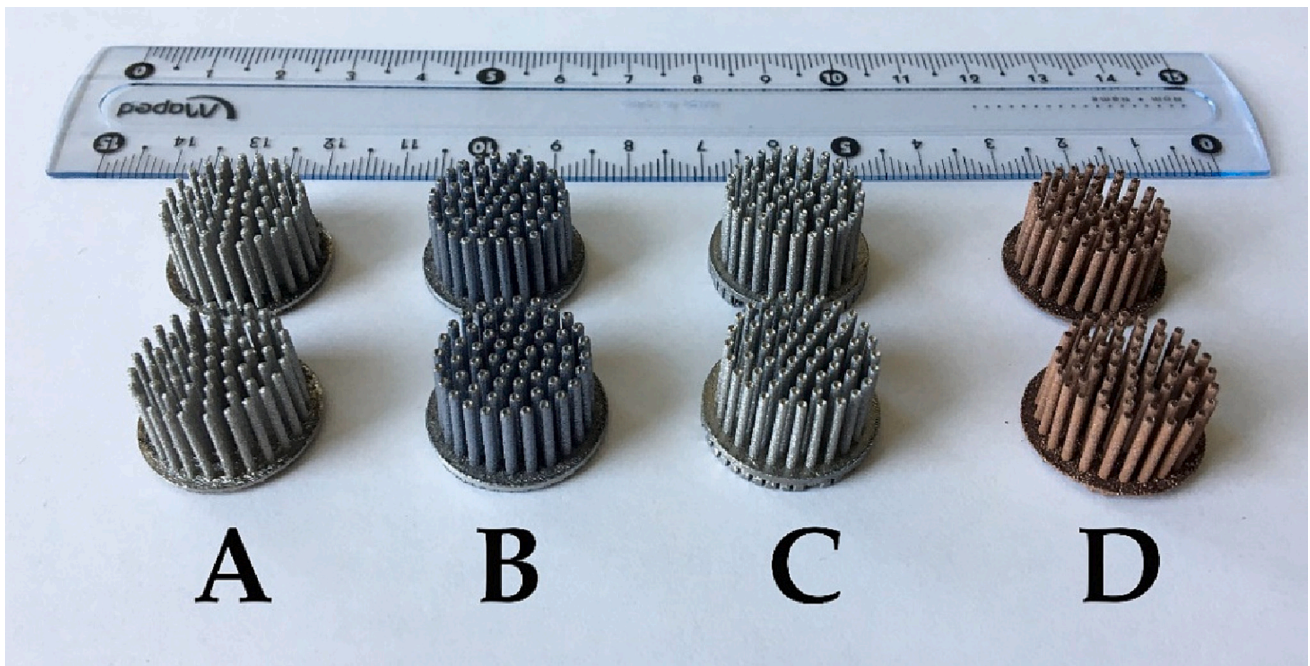


Fig. 4. SLMed cylindrical heatsink: A) Iron-based 316 L, B) Aluminum-based AlSi10Mg, C) Titanium-based Ti6Al4V, and D) Copper-based CuNi2SiCr. A solid plate with 1 mm thickness at the bottom (named spacer) connects printing supports to fins. The diameter of cylindrical fins/columns is 20 mm.

Table 2

The density of heatsinks is measured by the Archimedeian immersion method (ASTM D792). The mass density of powders is provided by producer’s data sheet on alloy’s chemical composition. The average roughness (R_a) for as-built structures was reported by the producer (ASTM B348).

Metallic heatsinks	Mass density (g/cm ³)	Heatsink density (g/cm ³)	Average roughness (μm)
316 L	7.98	7.946	8
AlSi10Mg	2.67	2.652	8
Ti6Al4V	4.43	4.418	14
CuNi2SiCr	8.84	8.724	15

characterization. Cylindrical pin fins were chosen for the micro-CT investigation rather than rectangular plate fins (comparing Figs. 5C and 6C) because of difficulties during the processing (small overlapping volume and cross-sectional area) and post-processing (with polishing and jet cleaning and scanning strategies). The AM 316 L fins fabricated using the SLM process have the lowest porosity level (99.76 % densified), as shown in Fig. 7 and Table 4. However, the Ti6Al4V structure has smaller pores/defects in terms of size/volume and AlSi10Mg has a smoother surface in the structure compared to 316 L (Fig. 7A), which is

Table 3

Powders, producers, and specifications. Note that the pure Cu, pure Ag and RBM-50C powders have branch flake, and polygon shape morphology, respectively.

Powder	Producer	Specification	Size
CuNi2SiCr	Eckart TLS GmbH, Germany	96.5 % copper balance and 2 % Ni	10–63 μm
RBM-50C	Van Moppes, Swiss	Diamonds, coated by 50 % copper	~40–50 μm
316 L	SLM Solution AG, Germany	Fe-balance, 17 % Cr, 12 % Ni, and 2 % Mo	10–45 μm
AlSi10Mg	SLM Solution AG, Germany	10 % Si, 0.3 % Mg and 0.5 % Fe	20–63 μm
Ti6Al4V	SLM Solution AG, Germany	Ti-balance, 6 % Al and 4 % V	20–63 μm
Ti22Al25Nb	Sino-Euro Ltd., China	Ti-balance, 22 % Al and 25 % Nb	15–45 μm
Pure Cu	Sigma-Aldrich, USA	99.5 % metal balance	~10–50 μm
Pure Ag	ABCR GmbH, Germany	99.95 % purity	$\leq 100 \mu\text{m}$

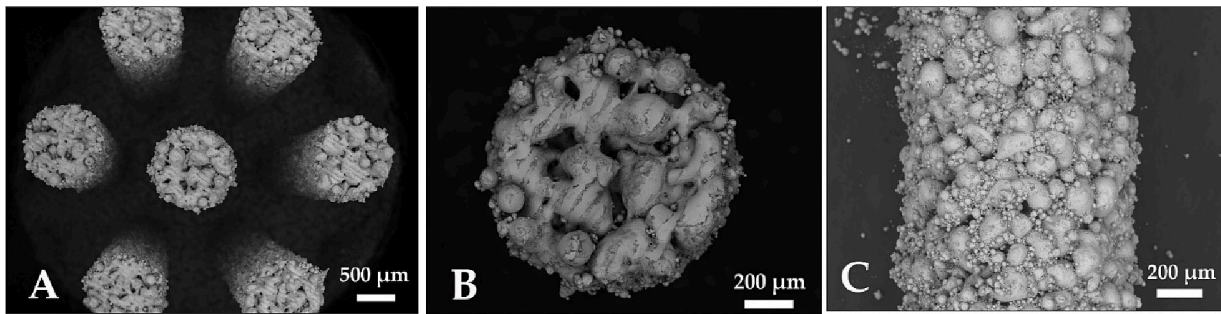


Fig. 5. A) Top view of cylindrical heatsink pin fins of CuNi2SiCr, B) Top view (cross-section) of a pin, and C) lateral view of the pin.

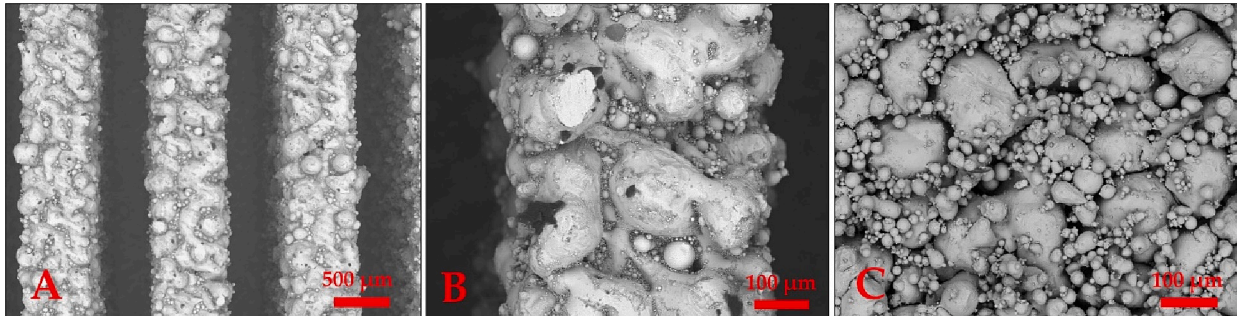


Fig. 6. A) Top view of rectangular heatsink plate fins of CuNi2SiCr, B) Top view (cross-section) of a plate, and C) lateral view of the plate.

because of melting of all particles during the SLM process (no stuck/un-molten/raw particles for AlSi10Mg). Note that the average particle size of Al-based alloy is relatively larger than Fe-based alloy as well as the thermal conductivity of aluminum, but the average of mean roughness for both is reported by the producer to be $\sim 8 \mu\text{m}$ as-built (see Table 2). Therefore, this lightweight structure (Fig. 7C) with smooth fins with insignificant changes in SLMed layers, shows a good agreement with the CAD model, which makes it a great candidate for aerospace applications compared to the traditional casting counterparts [24,25]. On the other hand, the Ti6Al4V structure (Fig. 7E and F) has many pores, but small in size/volume and uniform in distribution. Nevertheless, these pores are not likely to affect the strength of the heatsinks (smallest in 4 selected alloys, see Table 4), as found by Rezapourian et al. [26]. However, because of the cracking susceptibility, ultra-high thermal conductivity, and use of the infrared wavelength range, the CuNi2SiCr heatsink has the highest porosity and lowest densification level. In addition, the movement of the laser from left to right leads to the increase in porosity color contours, which shows the effect of heat conductivity during SLM scanning (Fig. 7G and H). It is worth mentioning that 3D-printing of copper and its alloys is a challenging task and is still under intensive development [27].

There are two main points that can be presented here; firstly, the addition of diamond particles (diamond particles coated with copper for better adhesion with copper structure, see Table 3 for RBM-50C powder) to fill the volume porosity of the structure, increase the strength and decrease the weight (Cu-Di composite). Secondly, the comparison of the SLM process (as an AM process with the ability to fabricate complex geometries) with the SPS process (as a PM process with the ability to process a wide range of materials). It is worth mentioning that plasma sintering provides one of the best densifications among the PM techniques and can be used as a benchmark for Cu-Di hybrid composites [28]. On the other hand, AM is a method that allows the diamond particles to be positioned at an exact/arbitrary location on the lattices, scaffolds, fins, and struts of complex shapes [29,30].

Fig. 8 shows sintered Cu-Di composites with different diamond content (after polishing), and the corresponding XRD patterns are shown

in Fig. 9. In Fig. 9A, no trace of carbon or graphite and small amount of diamond in the composition is detected. Additional phases, such as 0.6 % copper nitride and 1.3 % copper silicon are observed. Fig. 9B shows the XRD pattern of a sintered Cu-Di composite with 5.7 % graphite, while in Fig. 9C (which shows the hardest sample) is free of graphite or other copper compositions. To measure the Young's modulus, all samples were polished on both sides to obtain an identical height (1/3, 1/2, and 2/3, see Fig. 10A, B and C samples), as shown in Table 5 along with applied temperature and measured densities.

The samples of hybrid Cu-Di composites fabricated through SPS are presented in Fig. 8, where they have undergone coarse polishing. Fig. 10 shows the same samples after fine polishing. The Cu-Di samples in Fig. 10 were mechanically fine-polished to illustrate the ability of survival of diamond particles during polishing (simulating the abrasive medium for bonding of Cu and Di). Comparing Figs. 10 A–C shows that increasing the amount of diamond in a composite increases the probability of separation. This separation (weak bonding strength) for sample Fig. 10B appeared only for small particles, while it also occurred for larger particles for sample C. Coarse polishing (Figs. 8 A–C) was applied for the distribution of Di particles in the composite, which is important because of the difference in density of Di and Cu, and “positioning in-situ” during the 3D printing process. Fine polishing is one approach to test the adhesion of copper-diamond composite, either SLMed or SPSed. A lower amount of diamond content in the Cu-Di composite means less separation (either for bulk-sintered, or lattice-printed samples) and a higher possibility of 3D printing (positioning of Di in-situ particles).

It is important to clarify that the present article is discussing the benefits and drawbacks of both SLM and SPS techniques in relation to their combination, rather than presenting a comparative overview. Our ultimate objective was to create a copper-diamond (Cu-Di) composite, and through the utilization of SLM-SPS methods, in absence of binder jetting or green laser printing. This is particularly significant because it allows for the incorporation of hard materials like diamond particles into a porous metallic structure, which is not feasible with green laser technology.

The present paper aimed to form and localize hard materials, such as

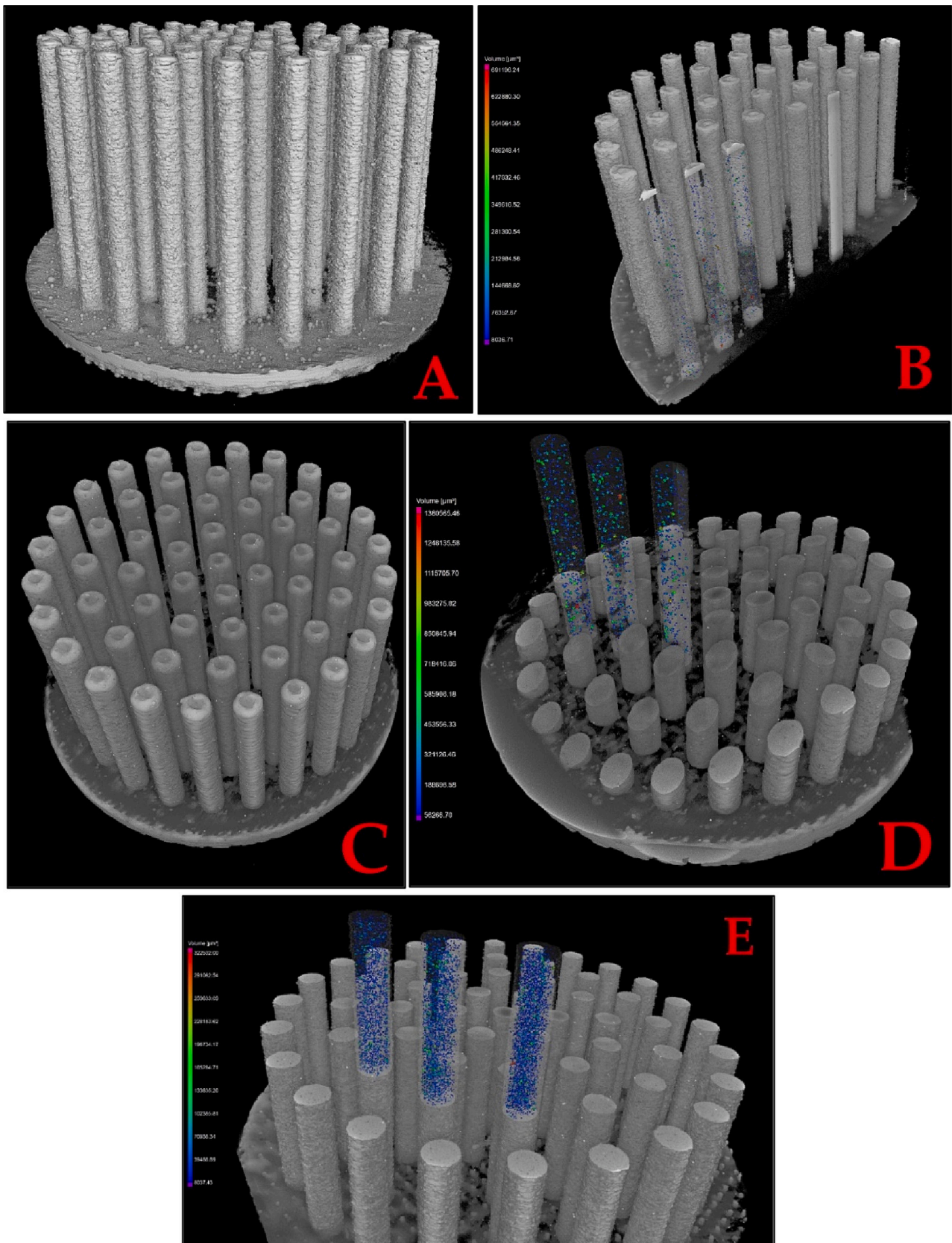


Fig. 7. Micro-CT scanning of cylindrical heatsinks from four different metallic alloys: A and B) 316 L; C and D) AlSi10Mg; E and F) Ti6Al4V; G and H) CuNi2SiCr. Color contours show the porosity in the fins.

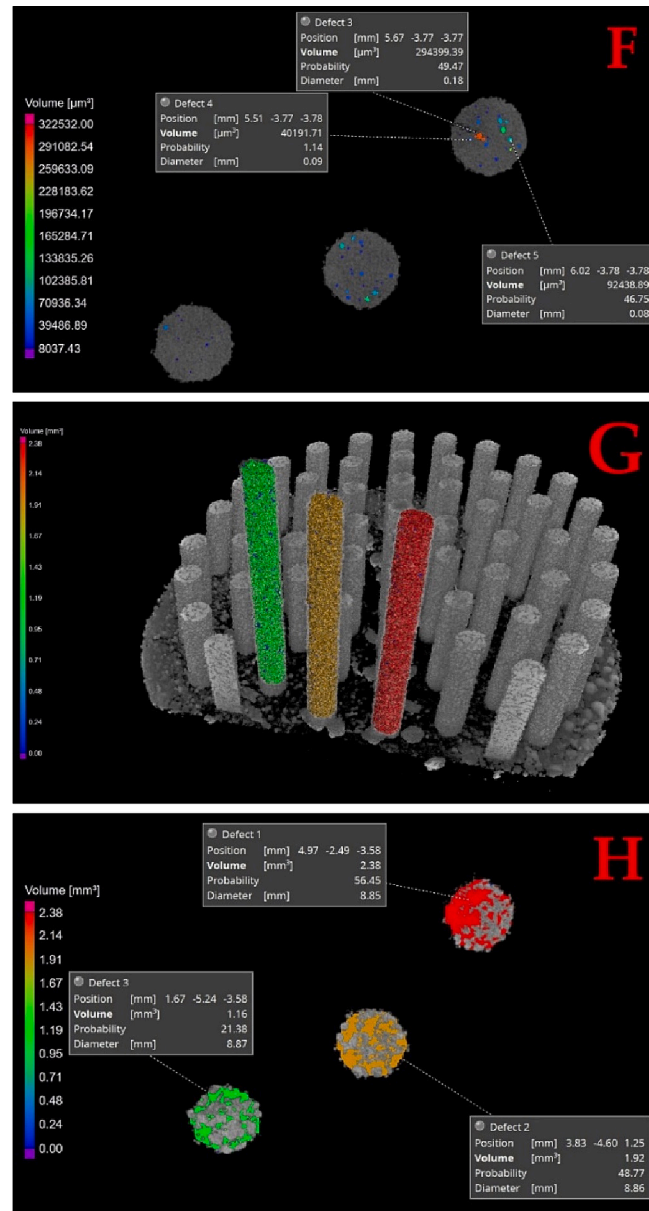


Fig. 7. (continued).

Table 4
CT scanning results of SLM fabricated heatsinks of various metal alloys.

Metallic alloys	Porosity level (%)	Maximum defect volume (mm ³)
316 L	~0.24	~7.0E-04
AlSi10Mg	~0.69	~1.4E-03
Ti6Al4V	~1.98	~3.0E-04
CuNi2SiCr	~26.58	~2.4E+00

diamond, within a copper lattice structure. However, assessing the electrical and thermal conductivity of such complex shapes would be a significant undertaking. The main difficulty lies in accurately measuring the lattice scaffolds rather than the bulk structures. Constantin et al. [31] demonstrated that laser 3D printing of pure Copper (95 % Cu) with a moderate laser power (400 W) resulted in a thermal conductivity of 368 Wm⁻¹.K⁻¹, comparable to that of bulk Cu, while printing complex heat sink structures with large surface areas (600 mm²/g). It was applied for high-efficiency cooling of electronic chips. Also, Lingqin et al. [32] reports pure copper in bulk form fabricated through SLM can achieve a

thermal conductivity of 377 Wm⁻¹.K⁻¹ (laser power of 500 W and layer thickness of 30 μm), which is 23 times higher than the thermal conductivity of 316 L built using the same method.

4. State of the art of Cu-Di 3D printing

This paper provides an overview of additively manufactured or sintered copper-balanced materials. The combination of powder metallurgy and powder bed fusion is a state-of-the-art approach, developed by the authors to simplify and reduce the costs of production. The distribution/layout of diamond particles (or other refractory materials) in favorable positions is done for porous/complex structures/scaffolds by SLM, and by a SLM-SPS combination for bulk structures.

Low-alloyed CuNi2SiCr (~96 % Cu balanced) and highly alloyed Cu15Ni8Sn (~75 % Cu balanced) are well-known powders used for SLM (Fig. 11). The first can be proposed as a wear resistant composite, while the second as an abrasive resistant compound with diamond particles. As one application, Yao et al. [33] reported deposition of CuNi2SiCr on a nickel-aluminum-bronze substrate with a grain size of ~100 μm to

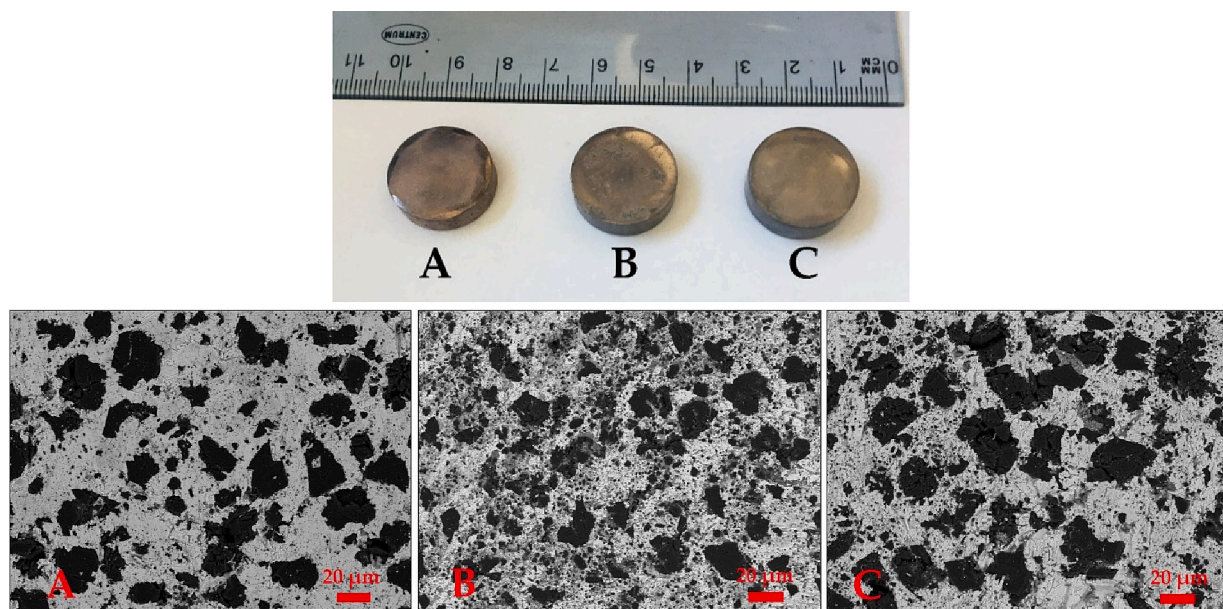


Fig. 8. Cu-Di composite with different diamond content after coarse polishing: A) Cu (10 g) and RBM-50C (5 g), approx. 17 % Di, B) Cu (7.5 g) and RBM-50C (7.5 g), approx. 25 % Di, and C) Cu (5 g) and RBM-50C (10 g), approx. 33 % Di.

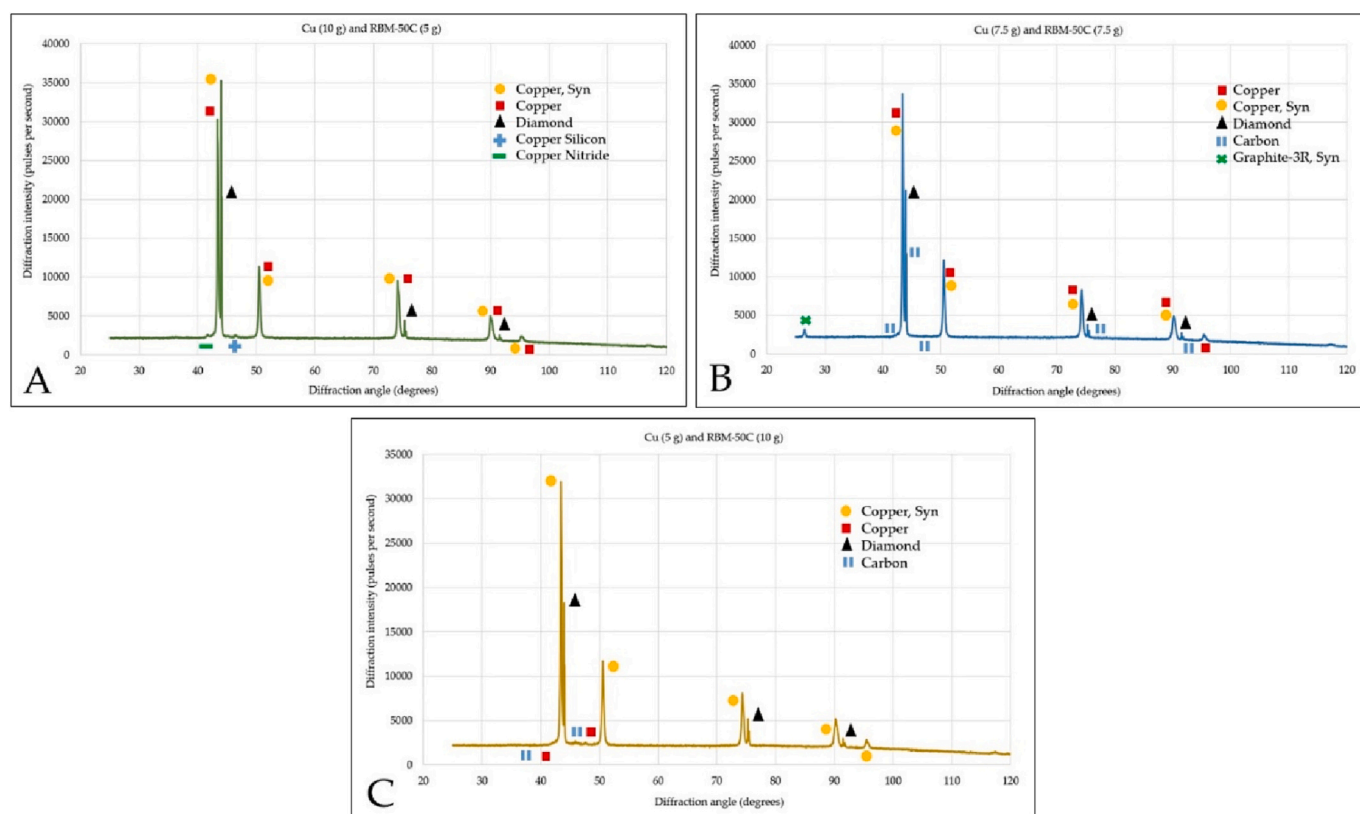


Fig. 9. XRD patterns of Cu-Di composite: A) Cu (10 g) and RBM-50C (5 g), B) Cu (7.5 g) and RBM-50C (7.5 g), and C) Cu (5 g) and RBM-50C (10 g).

repair the ship’s propellers using the directed energy deposition (DED) method, and to increase mechanical strength, reduced Sn separation, and improved processability Gao et al. [34] proposed adding 1 wt% TiB₂ to Cu15Ni8Sn. As widely reported in the literature, additive manufacturing is preferred over subtractive processes because it allows of the capability of the time- and cost-efficient fabrication of complex shapes fabrication, which is particularly emphasized in lattice and

scaffold structures [35,36]. As depicted in Fig. 12, the variation of the cell sizes (from 0.5 to 3 mm) and strut diameters (from 0.2 to 1 mm) can lead to new applications, e.g., impact absorption (wear resistance), compression resistance, hierarchical architecture, and lightweight/hybrid structure, etc. [37–39].

In addition to metal printing, ceramics [40], tribological materials [41], and multi-components materials (high-entropy alloys) [42] can

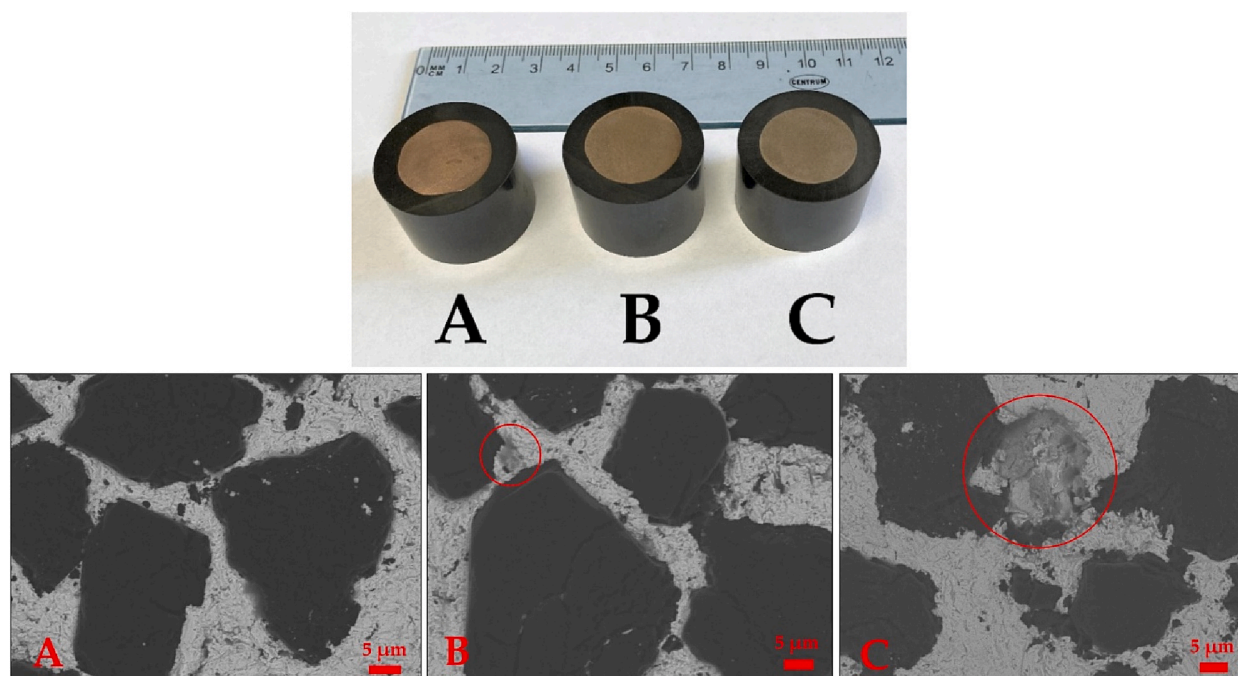


Fig. 10. Cu-Di composite with different content of diamond after fine polishing to simulate the abrasive medium: A) Cu (10 g) and RBM-50C (5 g), ~17 % Di, B) Cu (7.5 g) and RBM-50C (7.5 g), ~25 % Di, and C) Cu (5 g) and RBM-50C (10 g), ~33 % Di.

Table 5
Density and Young’s modulus of Cu-Di samples.

Bulk samples	Sample density (g/cm ³)	Young’s modulus (GPa)	SPS temperature (°C)
Cu pure	8.84	123	780
CuNi2SiCr	8.83	136	800
Cu-1/3 Di	7.14	198	780
Cu-1/2 Di	6.18	202	820
Cu-2/3 Di	5.33	180	860

also be individually realized using the SLM process, but the improvements of the mechanical properties for specific applications need further investigation. Surface (laser) texturing technologies for improving and developing novel heatsink designs (for improving thermal conductivity or heat dissipation) or bio-materials (for wear resistance) are very promising with respect to the current research on Cu-Di-based AM materials. Additionally, the application of such soft-metal/ceramic lattice

combinations can be beneficial in terms of improved flexibility and wear resistance concerning brushes, bearing bushes, and contact wires in electrical sliding [43]. The proposal for the fabrication of cermets (metal-ceramic composites) is to use integrated processes (see Fig. 2) starting with SLM for metallic matrix and continuing with SPS for the ceramic filling [44,45]. A concept design of CuNi2SiCr lattice printed by SLM and then filled with TiO₂-10 % Ag in SPS, is illustrated in Fig. 13. This concept and method can be applied to a wide range of metallic alloys (e.g., copper alloys) and ceramics (oxides or hard materials) associated with the specific applications [46–48].

5. Conclusion

In the present work, lattice structures were fabricated using the SLM process from low-alloyed copper, and the SPS technique was used to introduce diamond particles in these complex structures. The microstructural and mechanical properties, and pores morphology of fabricated hybrid composites containing hard particles with different content

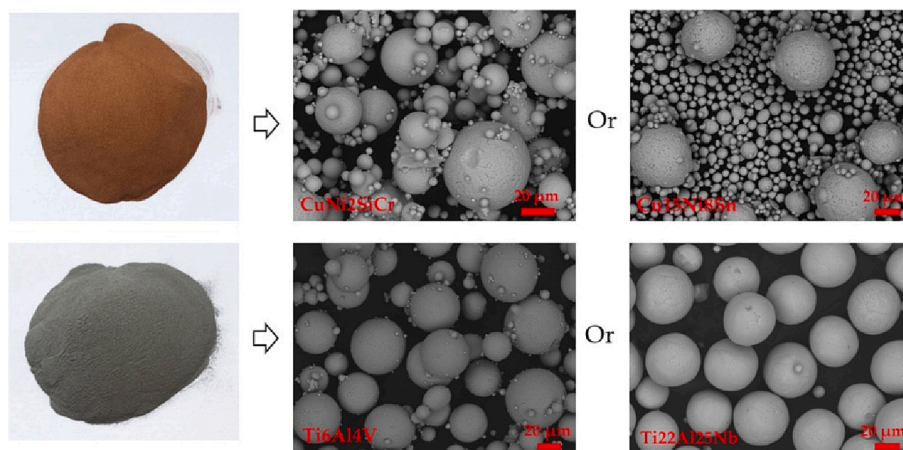


Fig. 11. Copper-based (Top, CuNi2SiCr, and Cu15Ni8Sn) and titanium-based (Bottom, Ti6Al4V, or Ti22Al25Nb) powders which are pre-alloyed for the SLM process. These powders with proportions of 70–90 % can mix with RBM-50C or RBM-50Ti.

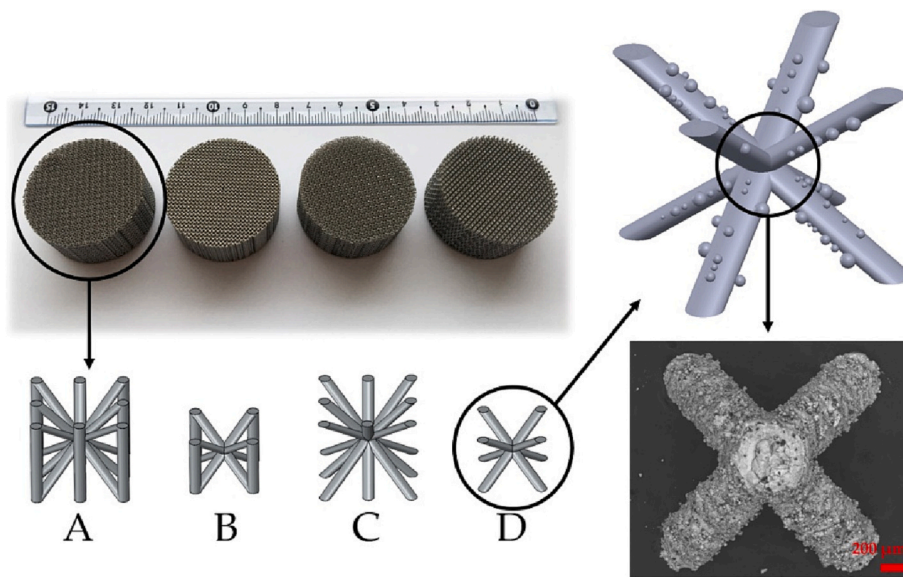


Fig. 12. Left: Ti6Al4V lattice structure design (Top, 30 mm diameter) based on different unit cells (Bottom); A) 16-struts BCC-Z $1.5 \times 1.5 \times 1.5 \text{ mm}^3$, B) 8-struts BCC-Z $1 \times 1 \times 1 \text{ mm}^3$, C) 8-struts BCC $1.5 \times 1.5 \times 1.5 \text{ mm}^3$, and D) 4-struts BCC $1 \times 1 \times 1 \text{ mm}^3$. Right: Realistic design of 4-cross sectional struts with inevitable unmelted/sticked powders (Top), and with the distribution of diamond particles throughout the struts (Bottom).

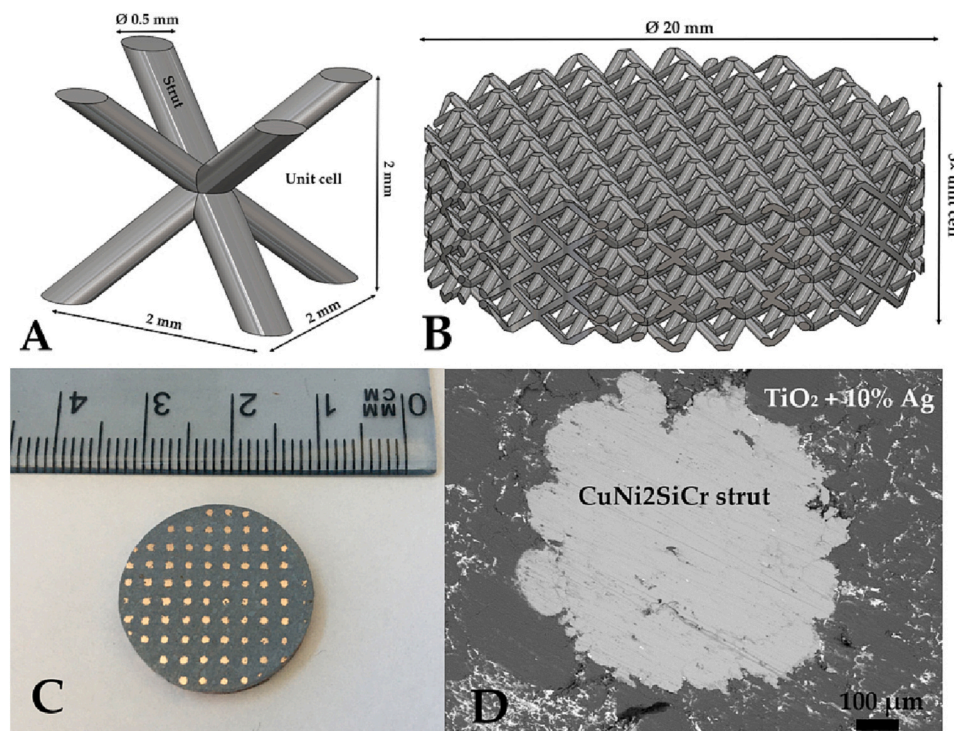


Fig. 13. A) Unit cell dimension, B) Lattice structure configuration, C) Photograph of CuNi2SiCr lattice (SLM-fabricated) filled by TiO_2 -10 % Ag (SPS-sintered), and D) SEM Micrograph of CuNi2SiCr lattice filled by TiO_2 -10 % Ag (metal-ceramic composite).

were investigated. The SPS process showed the possibility of localizing hard particles in the SLMed lattice structure, and the SPSed CuNi2SiCr filled with 1/2 content of diamond particles showed highest strength (202 GPa). The XRD studies showed no trace of graphite or other copper compositions for SPSed Cu-2/3Di composite (the hardest sample). The obtained results were compared with those fabricated complex heatsink structures using SLM from Fe- (316 L), Al- (AlSi10Mg), and Ti-based (Ti6Al4V), along with another Cu alloys (CuNi2SiCr), where the Fe-based alloys indicated the lowest porosity and Al-based alloys showed

finest surface structure. This fabrication method can be applied to combine a wide range of metallic alloys (e.g., copper and its alloys) and ceramics (e.g., oxides and hard materials) and fabricate multi-functional material –something that cannot be realized by the typical SLM process alone. The present results suggest that the materials with significant differences in their physical and mechanical properties can be used to fabricate complex structures using typical and available SLM and SPS machines, and these materials can be used in a wide range of industries, overcoming the limitations of the AM processes.

Author statement

The manuscript entitled “Fabrication of Localized Diamond-Filled Copper Structures via Selective Laser Melting and Spark Plasma Sintering” written by Ramin Rahmani, Javad Karimi, Nikhil Kamboj, Rahul Kumar, Miha Brojan, Adam Tchórz, Grzegorz Skrabalak, and Sérgio Lopes, is applied to the “Journal of Diamond and Related Materials” for peer review and publication. The authors declare that there are no conflicts of interest regarding this publication. The manuscript is original and has not been published in other journals or conferences.

CRedit authorship contribution statement

Conceptualization, R.R., and J.K.; methodology, R.R., and N.K.; investigation, R.R. and R.K.; experiments, R.R., and A.T.; writing—original draft preparation, R.R., J.K., N.K., and R.K.; writing—review and editing, M.B., G.S. and S.L.; supervision, G.S. and S.L. The authors declare no conflict of interest.

Declaration of competing interest

The authors declare that they have no known competing financial interests or personal relationships that could have appeared to influence the work reported in this paper.

Data availability

No data was used for the research described in the publication.

Acknowledgements

Ramin Rahmani acknowledges the support of NORTE-06-3559- FSE-000226, funded by Norte Portugal Regional Operational Program (NORTE 2020), under the PORTUGAL 2020 Partnership Agreement, through the European Social Fund (ESF). This work was also developed within the scope of the project ProMetheus – Research Unit on Materials, Energy and Environment for Sustainability, FCT Ref. UID/05975/2020, financed by national funds through the FCT/MCTES.

Javad Karimi would like to acknowledge the AiF German Federation of Industrial Research Associations (AiF-Forschungsvereinigung, IKAF, 01.3351).

Nikhil Kamboj acknowledges the support of Estonian Research Council (Project Number- PUTJD1169), and Academy of Finland Grant Number 325003 (Recovery of gold from the secondary resources by novel electrochemical reactors realized with additive manufacturing, ReGold-AM).

Rahul Kumar would like to acknowledge the M-ERA.Net project “DuplexCER”, funding of the “Austrian COMET-Programme” (Project InTribology1, no. 872176) under the scope of “K2 In Tribology” and collaboration of “Excellence Centre of Tribology” (AC2T research GmbH).

References

- G. Kasperovich, J. Haubrich, J. Gussone, G. Requena, Correlation between porosity and processing parameters in TiAl6V4 produced by selective laser melting, *Mater. Des.* 105 (2016) 160–170.
- M.X. Gan, C.H. Wong, Practical support structures for selective laser melting, *J. Mater. Process. Technol.* 238 (2016) 474–484.
- R. Rahmani, M. Antonov, L. Kollo, Y. Holovenko, K.G. Prashanth, Mechanical behavior of Ti6Al4V scaffolds filled with CaSiO₃ for implant applications, *Appl. Sci.* 9 (2019) 3844.
- M.F.F.A. Hamidi, W.S.W. Harun, N.Z. Khalil, M. Samykano, Microstructural comparison and mechanical properties of stainless steel 316L fabricated by selective laser melting and metal injection moulding processes, *Int. J. Manuf. Technol. Manag.* 33 (2019) 76–87.
- N. Soro, N. Saintier, H. Attar, M.S. Dargusch, Surface and morphological modification of selectively laser melted titanium lattices using a chemical post treatment, *Surf. Coat. Technol.* 393 (2020), 125794.
- Z.A. Munir, U.A. Tamburini, The effect of electric field and pressure on the synthesis and consolidation of materials: a review of the spark plasma sintering method, *J. Mater. Sci.* 41 (2006) 763–777.
- K. Dash, B.C. Ray, D. Chandra, Synthesis and characterization of copper-alumina metal matrix composite by conventional and spark plasma sintering, *J. Alloys Compd.* 516 (2012) 78–84.
- R. Rahmani, M. Antonov, L. Kollo, Wear resistance of (Diamond-Ni)-Ti6Al4V gradient materials prepared by combined selective laser melting and spark plasma sintering techniques, *Adv. Tribol.* 5415897 (2019).
- O. Guillon, J. Gonzalez-Julian, B. Dargatz, T. Kessel, G. Schiering, J. Räthel, Mathias Herrmann, Field-assisted sintering technology/spark plasma sintering: mechanisms, materials, and technology developments, *Adv. Eng. Mater.* 16 (2014) 830–849.
- M. Colopi, L. Caprio, A.G. Demir, B. Previtali, Selective laser melting of pure Cu with a 1 kW single mode fiber laser, *Procedia CIRP* 74 (2018) 59–63.
- T.-T. Keshoji, K. Nakamura, M. Yonehara, K. Imai, H. Kyogoku, Selective laser melting of pure copper, *JOM* 70 (2018) 396–400.
- T.Q. Tran, A. Chinnappan, J.K.Y. Lee, N.H. Loc, L.T. Tran, G. Wang, V.V. Kumar, W.A.D.M. Jayathilaka, D. Ji, M. Doddamani, S. Ramakrishna, 3D printing of highly pure copper, *Metals* 9 (2019) 756.
- K. Mizuuchi, K. Inoue, Y. Agari, S. Yamada, M. Tanaka, M. Sugioka, T. Takeuchi, J. Tani, M. Kawahara, J.H. Lee, Y. Makino, Thermal Properties of Diamond-Particle-Dispersed Cu-Matrix-Composites Fabricated by Spark Plasma Sintering (SPS), *Mater. Sci. Forum* 638–642 (2010) 2115–2120.
- T. Schubert, Ł. Ciupinski, W. Zielinski, A. Michalski, T. Weißgarber, B. Kieback, Interfacial characterization of Cu/diamond composites prepared by powder metallurgy for heat sink applications, *Scr. Mater.* 58 (2008) 263–266.
- R. Rahmani, K. Molan, M. Brojan, K.G. Prashanth, D. Stopar, High virucidal potential of novel ceramic-metal composites fabricated via hybrid powder bed fusion and powder metallurgy routes, *Int. J. Adv. Manuf. Technol.* (2022) 1–14.
- K. Molan, R. Rahmani, D. Krklec, M. Brojan, D. Stopar, Phi 6 bacteriophage inactivation by metal salts, metal powders, and metal surfaces, *Viruses* 14 (2022) 204.
- J. Chen, W. Hou, X. Wang, S. Chu, Z. Yang, Microstructure, porosity and mechanical properties of selective laser melted AlSi10Mg, *Chin. J. Aeronaut.* 33 (2020) 2043–2054.
- S.F. E. L. Shi, Z.G. Guo, W.M. Liu, The recent progress of tribological biomaterials, *Biosurf. Biotribol.* 1 (2015) 81–97.
- K. Zyglu, B. Nosek, H. Pasiowiec, N. Szysiak, Mechanical properties and microstructure of AlSi10Mg alloy obtained by casting and SLM technique, *World Sci. News* 104 (2018) 456–466.
- R. Kumar, I. Hussainova, R. Rahmani, M. Antonov, Solid lubrication at high-temperatures—a review, *Materials* 15 (2022) 1695.
- Y. Xiong, Y. Tang, S. Kim, D.W. Rosen, Human-machine collaborative additive manufacturing, *J. Manuf. Syst.* 66 (2023) 82–91.
- J. Maszybrocka, B. Gapinski, M. Dworak, G. Skrabalak, A. Stwora, Modelling, manufacturability and compression properties of the CpTi grade 2 cellular lattice with radial gradient TPMS architecture, *Bull. Pol. Acad. Sci. Tech. Sci.* 4 (2019) 719–727.
- R. Rahmani, M. Brojan, M. Antonov, K.G. Prashanth, Perspectives of metal-diamond composites additive manufacturing using SLM-SPS and other techniques for increased wear-impact resistance, *Int. J. Refract. Met. Hard Mater.* 88 (2020), 105192.
- C.-L. Yao, H.-S. Kang, K.-Y. Lee, J.-G. Zhai, D.-S. Shim, A study on mechanical properties of CuNi₂SiCr layered on nickel–aluminum bronze via directed energy deposition, *J. Mater. Res. Technol.* 18 (2022) 5337–5361.
- R. Rahmani, M. Antonov, K.G. Prashanth, The impact resistance of highly densified metal alloys manufactured from gas-atomized pre-alloyed powders, *Coatings* 11 (2021) 216.
- M. Rezapourian, N. Kamboj, I. Jasiuk, I. Hussainova, Biomimetic design of implants for long bone critical-sized defects, *J. Mech. Behav. Biomed. Mater.* 134 (2022), 105370.
- R. Rahmani, M. Antonov, L. Kollo, Selective laser melting of diamond-containing or postnitrided materials intended for impact-abrasive conditions: experimental and analytical study, *Adv. Mater. Sci. Eng.* 4210762 (2019).
- Q.L. Che, J.J. Zhang, X.K. Chen, Y.Q. Ji, Y.W. Li, L.X. Wang, S.Z. Cao, L. Guo, Z. Wang, S.W. Wang, Z.K. Zhang, Y.G. Jiang, Spark plasma sintering of titanium-coated diamond and copper–titanium powder to enhance thermal conductivity of diamond/copper composites, *Mater. Sci. Semicond. Process.* 33 (2015) 67–75.
- Z. Ren, D.Z. Zhang, G. Fu, J. Jiang, M. Zhao, High-fidelity modelling of selective laser melting copper alloy: laser reflection behavior and thermal-fluid dynamics, *Mater. Des.* 207 (2021), 109857.
- R. Velu, A.V. Kumar, A.S.S. Balan, J. Mazumder, Chapter 14 - laser aided metal additive manufacturing and postprocessing: a comprehensive review, in: *Additive Manufacturing (Handbooks in Advanced Manufacturing)*, 2021, pp. 427–456.
- L. Constantin, Z. Wu, N. Li, L. Fan, J.-F. Silvain, Y.F. Lu, Laser 3D printing of complex copper structures, *Addit. Manuf.* 35 (2020), 101268.
- X. Lingqin, C. Guang, Z. Luyu, L. Pan, Explore the feasibility of fabricating pure copper parts with low-laser energy by selective laser melting, *Mater. Res. Express* 7 (2020), 106509.
- C.-L. Yao, H.-S. Kang, K.-Y. Lee, J.-G. Zhai, D.-S. Shim, A study on mechanical properties of CuNi₂SiCr layered on nickel–aluminum bronze via directed energy deposition, *J. Mater. Res. Technol.* 18 (2022) 5337–5361.
- J. Gao, Q. Han, L. Wang, Z. Liu, S. Soe, Z. Zhang, Y. Gu, Laser powder bed fusion of TiB₂-modified Cu₁₅Ni₈Sn alloy: processability, microstructure and mechanical performance, *Mater. Sci. Eng. A* 855 (2022), 143879.

- [35] R. Rahmani, M. Antonov, N. Kamboj, Modelling of impact-abrasive wear of ceramic, metallic, and composite materials, *Proc. Est. Acad. Sci.* 68 (2019) 191–197.
- [36] M. Antonov, R. Ivanov, Y. Holovenko, D. Goljandian, R. Rahmani, L. Kollo, I. Hussainova, 3D printing of plain and gradient cermets with efficient use of raw materials, *Key Eng. Mater.* (2019) 239–245.
- [37] N. Kamboj, M.A. Rodríguez, R. Rahmani, K.G. Prashanth, I. Hussainova, Bioceramic scaffolds by additive manufacturing for controlled delivery of the antibiotic vancomycin, *Proc. Est. Acad. Sci.* 68 (2019) 185–190.
- [38] R. Rahmani, M. Brojan, M. Antonov, Lightweight 3D printed Ti6Al4V-ALSi10Mg hybrid composite for impact resistance and armor piercing shielding, *J. Mater. Res. Technol.* 9 (2020) 13842–13854.
- [39] S.F. Khosroshahi, S.A. Tsampas, U. Galvanetto, Feasibility study on the use of a hierarchical lattice architecture for helmet liners, *Mater.Today Commun.* 14 (2018) 312–323.
- [40] N. Kamboj, J. Kazantseva, R. Rahmani, M.A. Rodríguez, I. Hussainova, Selective laser sintered bio-inspired silicon-wollastonite scaffolds for bone tissue engineering, *Mater. Sci. Eng. C* 116 (2020), 111223.
- [41] Y. Holovenko, L. Kollo, M. Saarna, R. Rahmani, T. Soloviova, M. Antonov, K. G. Prashanth, S. Cygan, R. Veinthal, Effect of lattice surface treatment on performance of hardmetal-titanium interpenetrating phase composites, *Int. J. Refract. Met. Hard Mater.* 86 (2020), 105087.
- [42] J. Karimi, L. Kollo, R. Rahmani, P. Ma, Y.D. Jia, K.G. Prashanth, Selective laser melting of in-situ CoCrFeMnNi high entropy alloy: effect of remelting, *J. Manuf. Process.* 84 (2022) 55–63.
- [43] R. Kumar, M. Antonov, Y. Holovenko, A. Surzenkov, Erosive wear resistance of nature-inspired flexible materials, *Tribol. Lett.* 68 (2020) 51.
- [44] R. Rahmani, N. Kamboj, M. Brojan, M. Antonov, K.G. Prashanth, Hybrid metal-ceramic biomaterials fabricated through powder bed fusion and powder metallurgy for improved impact resistance of craniofacial implants, *J.Mater.* 24 (2022), 101465.
- [45] R. Rahmani, M. Rosenberg, A. Ivask, L. Kollo, Comparison of mechanical and antibacterial properties of TiO₂/Ag ceramics and Ti6Al4V-TiO₂/Ag composite materials using combining SLM-SPS techniques, *Metals* 9 (2019) 874.
- [46] Z. Ma, D.Z. Zhang, F. Liu, J. Jiang, M. Zhao, T. Zhang, Lattice structures of Cu-Cr-Zr copper alloy by selective laser melting: microstructures, mechanical properties and energy absorption, *Mater. Des.* 187 (2020), 108406.
- [47] J. Gan, H. Gao, S. Wen, Y. Zhou, S. Tan, L. Duan, Simulation, forming process and mechanical property of Cu-Sn-Ti/diamond composites fabricated by selective laser melting, *Int. J. Refract. Met. Hard Mater.* 87 (2020), 105144.
- [48] A. Ressler, N. Kamboj, M. Ledinski, A. Rogina, I. Urlić, I. Hussainova, H. Ivanković, M. Ivanković, Macroporous silicon-wollastonite scaffold with Sr/Se/Zn/Mg-substituted hydroxyapatite/chitosan hydrogel, *Open Ceramics* 12 (2022), 100306.